Hindawi
Applied Computational Intelligence and Soft Computing
Volume 2023, Article ID 7883177, 11 pages
https://doi.org/10.1155/2023/7883177

Research Article

Coordinate Control for an SMIB Power System with an SVC

Belkacem Kada [1] **and Ahmed K. Bensenouci** [2]

[1]*King Abdulaziz University, Aerospace Engineering Department, P.O. Box 80204, Jeddah 21589, Saudi Arabia*
[2]*King Abdulaziz University, Department of Electrical & Computer Engineering, P.O. Box 80204, Jeddah 21589, Saudi Arabia*

Correspondence should be addressed to Belkacem Kada; bkada@kau.edu.sa

Received 18 September 2022; Revised 15 November 2022; Accepted 15 February 2023; Published 17 April 2023

Academic Editor: Upaka Rathnayake

To improve power quality in power systems vulnerable to current disturbances and unbalanced loads, a hybrid control scheme is proposed in the present paper. A hybrid adaptive robust control strategy is devised for an SMIB power system equipped with a static VAR compensator to ensure robust transient stability and voltage regulation (SVC). High-order sliding mode control is combined with a dynamic adaptive backstepping algorithm to form the basis of this technique. To create controllers amenable to practical implementation, this method uses a high-order SMIB-SVC model and introduces dynamic constraints, in contrast to prior approaches. Improved transient and steady-state performances of the turbine steam-valve system are the goals of the dynamic backstepping controller. A Lyapunov-based adaptation law is developed to address the ubiquitous occurrence of parametric and nonparametric uncertainty in electrical power transmission systems due to the damping coefficient, unmodeled dynamics, and external disturbance. High-order sliding mode (HOSM) control is used for generator excitation and SVC devices to construct finite-time controllers. The necessary derivatives for HOSM control are calculated using high-order numerical differentiators to prevent simulation instability and convergence issues. Simulations demonstrate that the suggested method outperforms conventionally coordinated and hybrid adaptive control schemes regarding actuation efficiency and stability.

1. Introduction

Today's power systems are far more loaded than in the past and are frequently operated at capacity, resulting in technical constraints, equipment deterioration, and economic losses. Load changes, transmission line outages, and short circuits continue to be the typical operating conditions that cause generators to experience poorly damped oscillations, loss of synchronism, and instability. Designing adequate control methods is one of the most effective strategies to address these difficulties. Stability and voltage management of power systems are critical, particularly for long transmission lines and large power plants [1, 2].

Single-machine infinite bus (SMIB) is a crucial technology for real-time voltage management and stability. It helps improve dependability, stability, and transmission efficiency. The coordination between SMIB and shunt-type flexible alternating current transmission systems (FACTSs), such as static VAR compensator (SVC) provides suitable control solutions for their interdependent parameters. Since 1970, SVC technology has been used as a realistic solution to the problem of continually generating or absorbing reactive power, and it is still utilized in AC power systems. SVC devices can exchange capacitive or inductive currents. The integrated SMIB-SVC system provides effective frequency oscillation damping, enhances transient stability, and controls the voltage and reactive power [3]. However, the complexity of modern power systems complicates and challenges the design of coordinated controllers for SMIB-SVC.

Modern power systems improve high-order multivariable processes that involve highly nonlinear electrical elements and parametric uncertainty. Changes in their inherent nonlinear properties are frequently time-varying, rendering fixed-parameter control algorithms incapable of delivering sufficient performance. Therefore, high-order dynamic models and adaptive parameter update laws are required for the control design. Adaptive

robust control is crucial to appropriately compensate for nonlinear dynamics, fast unmodeled dynamics, and disturbances. However, several signal processing-related technical challenges arise when designing adaptive controllers, and designers must consider all settings and variables when working in an industrial environment. Much research has been devoted to developing adaptive generator excitation and steam-valve controllers in recent years. For example, Wan et al. [4] designed a nonlinear SMIB-SVC controller using the immersion and invariance (I&I) approach. The authors implemented class-K functions to improve transient and steady-state performance. Milla and Duarte-Mermoud [5] created a predictive optimization adaptive (POA) method for computing PSS device parameters. The oscillations of the SMIB were enhanced by the POA-PSS method. Liu et al. [6] suggested a continuing fraction-based method for online simulation and control of power systems using SMIB. Bux et al. [7] examined the damping effect of the VSC stabilizer and its influence on electromechanical oscillation modes. To compensate for parameter sensitivity in SMIB, Roy et al. [8] integrated feedback linearization with adaptive control. The control strategy based on Lyapunov was superior to previous exciting partial feedback linearizing schemes. Kamari et al. [9] presented an optimal PSS-PID controller for suppressing low-frequency oscillations in SMIB. Using a PID controller, the authors tuned the controller's parameters using chaotic practical optimization (CPSO). CPSO-PID effectively minimized overshooting and decreased the transient response's settling time. Mijbas et al. [10] presented the multiobjective particle swarm optimization (PSO) technique to enhance the generator's power angle stability. They demonstrated that changing the controller parameters using PSO improves the stability of the SMIB-SVC system. Kumar et al. [11] utilized ACO-based SSSC to attenuate low-frequency oscillations and voltage variations in multimachine power networks. SSC effectively eliminated interarea subsynchronous oscillations and voltage variations by adopting ACO-based control with the voltage source. Muhammad et al. [12] optimized PSS parameters using the PSO algorithm. The perfect performance of PSS ensured the stability of the SMIB rotor's frequency response and power angle. However, the probabilistic character of population-based approaches may result in a loss of precision due to overestimating control benefits. Recently, linearized model-based techniques, such as optimum control and direct adaptive control, have been employed to provide high bandwidth and resilient performance in the presence of uncertainties (see [13–17]). Meanwhile, adaptive robust control design sometimes requires more than a linearized system model can provide.

High-order sliding mode (HOSM) control is gaining popularity in building resilient power network controllers due to load disturbances and measurement noises. Wan and Jiang [18] created a super-twisting sliding model-based control strategy for SMIB to provide robust stability and high-performance control. Han and Liu [19] designed a control technique for perturbed triple integrator chains using HOSM control. Trip et al. [20] designed a load frequency controller for power networks using sliding mode control of the second order. Although the controller displayed excellent tracking performance, it could not adequately adjust for frequency measurement disturbances. Adirak and Ekkachi [21] combined backstepping control and first-order sliding mode control to improve the transient stability and voltage regulation of SMIB. Compared to I&I and conventional backstepping control, the suggested control method demonstrated appropriate performance and enhanced closed-loop control stability. Neither external disturbances nor measurement noises were accounted for in this system. Under load disturbances, Dev et al. [22] proposed an adaptive super-twisting sliding mode controller for two sections of interconnected power networks. The authors implemented the dynamic adaptive rule proposed by Gutierrez et al. [23] to deal with the unknown limits of disturbances and prevent overestimating control advantages.

This study presents a novel solution to the problem of transient stability and voltage regulation in power systems with an SVC device. An SMIB-SVC backstepping-HOSM coordinated control technique is intended to simultaneously regulate the synchronous generator and SVC device. The nonlinear coordinated control of SMIB-SVC has received only a few important contributions until recently. Using a simplified SMIB-SVC model, Kanchanaharuthai and Mujjalinvimut [24] suggested a nonlinear coordinated control approach resembling backstepping. The authors demonstrated that their design methodology outperforms I&I control and conventional backstepping techniques. To recover the output voltage and remove power angle variations, Psillakis and Alexandridis (2020) utilized backstepping and feedback linearization control approaches. Keskes et al. [25] created a nonlinear coordinated control for the SMIB-SVC by employing input-output linearization and pole-assignment techniques. The authors demonstrated that the suggested control scheme outperformed traditional PSS and noncoordinated controllers regarding oscillation damping and voltage regulation. As with most known design methods, these control algorithms are unrestricted, fulfill asymptotic stability, and frequently exhibit a chattering effect that is difficult to implement in practice.

This study stands out in comparison to similar ones conducted recently. The following are the principal contributions of the current paper. It starts with an eighth-order mathematical model of the SMIB-SVC system. A high-order SMIB-SVC model is required to improve transient and steady-state performance. The dynamics of mechanical power, exciter dynamics, and SVC dynamics are all considered in the model, as are the impacts of subflux and transitory flux couplings along the d and q axes. This model is a significant improvement over its predecessors in the literature when applied to power

systems that are inextricably linked to one another (e.g., [4, 9, 18, 25, 26]). Second, a dynamically constrained backstepping (ADBS) controller is developed to enhance steady-state performance and attain transient stability. Third, parameter uncertainties and insufficiency in load disturbance compensation are addressed by adding a Lyapunov-based adaptation law to the load controller. Fourth, the synchronous generator and SVC device are controlled in tandem using controllers based on the finite-time HOSM model. The suggested ADBS-HOSM control strategy ensures more enhanced transient stability, decreased susceptibility to parameter uncertainties, and resilience against disturbances and measurement noises compared to recent contributions (e.g., [4, 18, 25]). Furthermore, the ADBS-HOSM control is chattering-free, shielding the actuators from the erratic high-frequency oscillations induced by feedback linearization and traditional sliding mode controllers. According to the authors, this is the first citation for finite-time backstepping-HOSM coordinated control design based on a comprehensive SMIB-SVC model.

The paper is formatted as follows: Section 2 explains an enhanced dynamic SMIB-SVC model. Section 3 presents the design of the nonlinear backstepping controller and adaptive parameter law. Section 4 develops HOSM controllers for generator excitation and SVC devices. In Section 5, numerical simulations are performed to validate the theoretical conclusions and assess the performance of the suggested control approach. The conclusion is presented in Section 6.

2. Dynamic Modeling and Problem Statement

The control laws designed with the traditional third-order power system model in mind have been shown in the literature to be a common cause of power oscillations and instability. As a result, only control laws based on a high-order model can guarantee optimal transient and steady-state performance. Here, we provide a nonlinear eighth-order SMIB-SVC dynamic model that accounts for both parametric and nonparametric forms of uncertainty.

2.1. Mechanical Load Dynamics

$$\begin{cases} \dot{\delta} = \omega - \omega_0, \\ \dot{\omega} = -\dfrac{D}{H}(\omega - \omega_0) + \dfrac{\omega_0}{H}\left(P_m + C_{ML}P_{m_0} - P_e\right), \\ \dot{P}_m = \dfrac{(C_H - 1)}{T_H}P_{m_0} - \dfrac{1}{T_H}(P_m + C_H u_h), \end{cases} \tag{1}$$

where δ, ω, ω_0, P_m, P_e, and u_h denote the generator rotor angle, angular speed, synchronous speed, mechanical power input, active power, and governor value position. H, D, T_H, and C_H denote the inertia constant, damping coefficient, time constant, and throttle pressure.

2.2. Exciter Dynamics

$$\begin{cases} \dot{E}'_q = \dfrac{1}{T'_{d0}}\left(-E_q + \dfrac{(x_d - x'_d)V_s \cos\delta}{x'_{ds}} + V_F\right), \\ \dot{E}'_d = -\dfrac{1}{T_E}\left[\left(K_E + Ae^{BE_{fd}}\right)E_d - V_F\right], \\ \dot{R}_F = -R_F + \dfrac{K_F}{T_F}E_d, \\ \dot{V}_F = -\dfrac{1}{T_A}\left[-K_A R_F + \dfrac{K_A K_F}{T_F}E_d - K_A\left(V_{ref} - V_t\right) + V_F\right], \end{cases} \tag{2}$$

where E_q, E_d, E'_q, E'_d denote the q-axis and d-axis voltage and transient voltages, V_s, V_F, and V_t denote the infinite bus, field, and terminal voltages of the generator, respectively, T_E and K_E are the time constant and exciter parameter, x_d, x'_d, and x'_{ds} denote the d-axis generator, transient reactance, and equivalent transient reactance, respectively, T_{d0} and T'_{d0} are the time constants of the excitation winding, and A and B are positive constants.

2.3. SVC Dynamics

$$\dot{B}_{\mathrm{SVC}} = \frac{1}{T_c}\left(-B_{\mathrm{SVC}} + B_{\mathrm{SVC}_0}\right) + \frac{K_c}{T_c}u_B,$$

$$\begin{cases} P_e = E'_q V_s B_{\mathrm{SVC}} \sin(\delta), \\ B_{\mathrm{SVC}} = \dfrac{1}{X_1} + X_2 - X_1 X_2 (B_L - B_C), \\ X_1 = x'_d + x_T + x_{L_1}, \\ X_2 = x_{L_2}, \end{cases} \tag{3}$$

where B_{SVC_0}, T_c, K_c, and u_B denote the initial susceptance, time constant, gain, and the equivalence output of the SVC controller, x_{L_1} and x_{L_2} are the reactance of the transmission lines, x_T denotes the transformer reactance, and B_L and B_C are the susceptance of the inductor of TCR (i.e., thyristor-controlled reactor) and the susceptance of the capacitor in SVC, respectively (see [26, 27]). Model (1)–(3) presents a complete and more accurate SMIB-SVC model that can be used in designing advanced controllers. It is worth noting that since the power system has an SVC electronic compensator, its d-axis equivalent reactance is time-varying even in the absence of disturbances.

3. Dynamic Feedback Backstepping for Load Control

3.1. Load Control Model Parametrization. For designing a dynamic adaptive backstepping load controller, dynamics (1) are described in a parametric form, with $P_e = E'_q V_s / x'_d \sin\delta$, as follows:

$$\dot{\mathbf{x}} = \mathbf{f}(\mathbf{x}, \boldsymbol{\theta}) + \mathbf{g}(\mathbf{x})\mathbf{u} + \mathbf{d}(\mathbf{x}, t), \tag{4}$$

with

$$\begin{aligned}
\mathbf{x} &= \begin{bmatrix} x_1 & x_2 & x_3 \end{bmatrix}^T \\
&= \begin{bmatrix} \delta - \delta_0 & \omega - \omega_0 & P_m - P_{m_0} \end{bmatrix}^T, \mathbf{f}(\mathbf{x}, \boldsymbol{\theta}) \\
&= \begin{Bmatrix} x_2 \\ -\theta_1 x_2 + \dfrac{\omega_0}{H} x_3 - \theta_2 \omega_0 \sin(x_1 + \delta_0) + \dfrac{\omega_0 P_{m_0}(C_{CL} + 1)}{H} \\ -\dfrac{1}{T_H} x_3 + \dfrac{1}{T_H}(1 - C_H) P_{m_0} \end{Bmatrix}, \\
\mathbf{g} &= \begin{bmatrix} 1 & \dfrac{\omega_0}{H} & -\dfrac{C_H}{T_H} \end{bmatrix}^T, \mathbf{u} = \begin{bmatrix} x_2^* & x_3^* & u_h \end{bmatrix}^T,
\end{aligned} \tag{5}$$

where x_2^* and x_3^* denote some fictive controls and $\mathbf{d}$ represents the external disturbance. The state x_1 is selected to be the tracked output. Model (4) is parameterized using the following vector θ:

$$\boldsymbol{\theta} = \begin{bmatrix} \theta_1 & \theta_2 \end{bmatrix}^T = \begin{bmatrix} \dfrac{D}{H} & \dfrac{E_q' V_s}{(H x_d')} \end{bmatrix}^T. \tag{6}$$

The control vector $\mathbf{u}$ is designed to asymptotically drive the states to their zero level despite parameter uncertainties and disturbances. The output $y = x_1$ is subjected to the following asymptotically stable constraints:

$$\ddot{x}^c(t) + \alpha_1 \dot{x}^c(t) + \alpha_2 x^c(t) = 0, \tag{7}$$

where $\alpha_1, \alpha_2 \in \mathscr{R}^+$. The control input $\mathbf{u}$ must guarantee a satisfactory performance level and maintain a sufficient robustness margin under the following assumptions:

Assumption 1. The functions $\mathbf{f}$ and $\mathbf{g}$ are uncertain functions due to the uncertainties of the parameters x_d' and D.

Assumption 2. The uncertainties $\Delta\mathbf{f}$ and $\Delta\mathbf{g}$ have bounded Euclidian norms: $\|\Delta\mathbf{f}\|_2 < \mu_1$ and $\|\Delta\mathbf{g}\|_2 < \mu_2$ with $\mu_1, \mu_2 \in \mathscr{R}^+$.

Assumption 3. The nonparametric disturbance $\mathbf{d}$ satisfies that $\|\mathbf{d}\|_2 < d_{\max} \in \mathscr{R}^+$.

Assumption 4. The control input $\mathbf{u}$ is a Lebesgue measurable bounded signal.

Assumptions 1 and 2 are made according to the requirements of control-affine nonlinear systems (i.e., nonlinear dynamics systems with a linear control input), which is consistent with the proposed nonlinear backstepping control type. In adaptive nonlinear-affine control theory, the functions $\mathbf{f}(\mathbf{x})$ and $\mathbf{g}(\mathbf{x})$ must be smooth and bounded, with a known local relative degree to the control input u. Numerous control designs, including backstepping, feedback linearization, and sliding mode control techniques, require such assumptions [28].

For Assumption 3, external disturbances and parameter uncertainties are inevitably present in power systems, including SMIB systems. They are typically unknown and unmeasurable, drastically degrading the desired control's performance. Observers must be designed with disturbance rejection or compensation. In such observers' design, the upper limit of the disturbance must be specified. The practical applicability of the designed control law is contingent on the fourth assumption. A Lebesgue measurable function must represent an admissible signal control. The Lebesgue condition ensures that the control law has a physical meaning and is applicable [29].

3.2. Backstepping Controller Design. We consider the parametric model (4) as a cascade connection of three subsystems (8) and define, for each subsystem, a candidate Lyapunov function (CLF), as shown in (9),

$$\begin{cases} \dot{x}_i = f_i(\mathbf{x}, \boldsymbol{\theta}) + g_i u_i + d_i(\mathbf{x}, t), \\ y_i = x_i^c, \end{cases} \tag{8}$$

$$V_i(\mathbf{e}) = \frac{1}{2} \sum_{j=1}^{i} e_j^2, \tag{9}$$

where $\mathbf{e} = \begin{bmatrix} e_1 & e_2 & e_3 \end{bmatrix}^T$ denotes the state error vector with $e_j = (x_j - x_j^c)$ and x_j^c being the expected states of the model (4).

Theorem 1. *Let Assumptions 1–4 hold. The output of model (4) asymptotically converges to its reference value under the dynamic constraints (7) if the effective control input* u_h *is chosen as*

$$u_h(\mathbf{x}, \boldsymbol{\theta}) = \boldsymbol{\Lambda}\mathbf{e} - \varphi(\mathbf{f}) - \phi(\mathbf{d}) - \chi(x_1^c), \tag{10}$$

and the control gains are appropriately selected such that $k_1, k_2, k_3 \in \mathscr{R}^+$ *with*

$$\begin{aligned}
\boldsymbol{\Lambda} &= \begin{bmatrix} \dfrac{-k_1^3}{g_1 g_2 g_3} & \dfrac{k_1^2 + k_1 k_2 + k_2^2}{g_2 g_3} & \dfrac{-(k_1 + k_2 + k_3)}{g_3} \end{bmatrix}^T, \\
\varphi(\mathbf{f}) &= \frac{\ddot{f}_1}{g_1 g_2 g_3} + \frac{\dot{f}_2}{g_2 g_3} + \frac{f_3}{g_3}, \\
\phi(\mathbf{d}) &= \frac{\ddot{d}_1}{g_1 g_2 g_3} + \frac{\dot{d}_2}{g_2 g_3} + \frac{d_3}{g_3}, \chi(x_1^c) \\
&= \frac{1}{g_1 g_2 g_3} \left[\left(\alpha_1^2 - \alpha_2 \right) \dot{x}_1^c + \alpha_1 \alpha_2 x_1^c \right].
\end{aligned} \tag{11}$$

Proof. The control law (10) is designed using recursive dynamic backstepping. To do so, we consider the following three-step stabilizing scheme. □

Step 1. As a starting step, a virtual state feedback law $x_2^*(\mathbf{x}, \theta)$ is sought to stabilize the first subsystem asymptotically. This is done if there exists a specific gain $k_1 \in \mathscr{R}^+$ that fulfills the following inequality:

$$\dot{V}_1(e_1) \leq -k_1 e_1^2. \tag{12}$$

Substituting $e_1 = (x_1 - x_1^c)$ in expression (12) gives

$$\dot{V}_1(e_1) = e_1 \dot{e}_1 = e_1(\dot{x}_1 - x_1^c) \leq -k_1 e_1^2. \tag{13}$$

Using the first equation of model (4), one can find that the condition (13) is guaranteed by the following virtual control x_2^*:

$$x_2^* = -\frac{[k_1(x_1 - x_1^c) + f_1 + d_1 - \dot{x}_1^c]}{g_1}. \tag{14}$$

It is clear that the intermediate control law (13) asymptotically steers x_1 towards x_1^c for a selected gain k_1.

Step 2. Similarly, it can be easily proven that there exists a gain $k_2 \in \mathscr{R}^+$ for which

$$\dot{V}_2(e_1, e_2) < -k_1 e_1^2 - k_2 e_2^2, \tag{15}$$

and with $\dot{e}_1 = g_1 x_2 - k_1 e_1 = g_1(e_2 + x_2^*) - k_1 e_1$, the second subsystem is asymptotically stable under the following virtual control:

$$x_3^* = -\frac{1}{g_2}\left[k_2 e_2 + f_2 + d_2 + \frac{\dot{x}_2^*}{g_1}\right] - \frac{1}{g_1 g_2}\left[+g_1 k_1 e_2 - k_1^2 e_1 + \dot{f}_1 + \dot{d}_1 + (\lambda_1 \dot{x}_1^c + \lambda_2 x_1^c)\right]. \tag{16}$$

The control law (16) guarantees the global asymptotical stability of the first and second subsystems. However, x_3^* is only a virtual control law, which implies the following step.

Step 3. The final step in the backstepping procedure is to find the accurate control input u_h under which the system (4) reaches its coordinate origin or operating point $(\delta_0, \omega_0, P_{m0})$ with desired performances and under prescribed dynamic constraints. Taking the time derivative of CLF V_3,

$$\dot{V}_3 = -k_1 e_1 - k_2 e_2 + e_3 \dot{e}_3 = -k_1 e_1 - k_2 e_2 + e_i(\dot{x}_3 - \dot{x}_3^*), \tag{17}$$

and then, with $\dot{e}_2 =$, if there exists a constant $k_3 \in \mathscr{R}^+$ such that

$$\dot{V}_3 < -\sum_{i=1}^{3} k_i e_i^2, \tag{18}$$

It results that the real control u_h is deduced from (4), (17), and (18) as defined in form (10).

This is the end of the proof.

Remark 1. The feedback control law (10) is nonsingular since $g_i(\mathbf{x}) \neq 0, i = 1, 2, 3, \ \forall \mathbf{x} \in \mathbb{X}$, where $\mathbb{X}$ denotes the operating space of model (4).

Remark 2. The case $\alpha_1 = \alpha_2 = 0$ corresponds to the unconstrained model.

3.3. Adaptive Dynamic Backstepping Controller. In Subsection 2.3, the backstepping controller (10) was derived under nominal conditions with known parameters θ_1 and θ_2. In practice, the values of these parameters change with the system's parameters. To introduce the uncertainties $\Delta\theta_i$, a new parameter error vector $\mathbf{e}_\theta = \theta - \widehat{\theta} = [\theta_1 - \widehat{\theta}_1 \quad \theta_2 - \widehat{\theta}_2]^T$ is defined with $\widehat{\theta}_1$ and $\widehat{\theta}_2$ being the estimators of θ_1 and θ_2, respectively. The uncertain form of the vector-valued function $\mathbf{f}$ in equation (4) is defined as follows:

$$\mathbf{f}(\mathbf{x}, \widehat{\boldsymbol{\theta}}) = \mathbf{h}(\mathbf{x}) + \boldsymbol{\Psi}(\mathbf{x})\boldsymbol{\theta} = \mathbf{h}(\mathbf{x}) + \boldsymbol{\Psi}(\mathbf{x})\left(\mathbf{e}_\theta + \widehat{\boldsymbol{\theta}}\right), \tag{19}$$

with

$$\mathbf{h}(\mathbf{x}) = \left[0 \ \frac{\omega_0 P_{m_0}(1 + C_{ML})}{H}\left(-\frac{1}{T_H}x_3 - \frac{1}{T_H}P_{m_0}\right)\right]^T, \boldsymbol{\Psi}(\mathbf{x}) = \begin{bmatrix} 0 & 0 \\ -x_2 & -\omega_0 x_4 \sin(x_1 + \delta_0) \\ 0 & 0 \end{bmatrix}. \tag{20}$$

Theorem 2. *Suppose that the unknown estimators $\widehat{\theta}_1$ and $\widehat{\theta}_2$ are bounded, the closed-loop control (19) is robustly stable under the law (21) conjointly with the parameter update law (22) if the vector $\mathbf{c}$ fulfills the output condition (23).*

The control law is

$$u_h(\mathbf{x}, \widehat{\boldsymbol{\theta}}) = \boldsymbol{\Lambda} e - \varphi(\widehat{\mathbf{f}}) + \boldsymbol{\Psi}(x)\widehat{\boldsymbol{\theta}} - \phi(\mathbf{d}) - \psi(x_1^c). \tag{21}$$

The adaptive law is

$$\dot{\widehat{\boldsymbol{\theta}}} = \Gamma \Psi_2 \mathbf{c}^T \mathbf{x}. \tag{22}$$

The output condition is

$$\mathbf{c}^T \mathbf{x} - e_2 < 0, \tag{23}$$

with $\Gamma = \mathrm{di\,ag}(\rho_1 \ \rho_2)$ and $\rho_i > 0$ denoting adaptive gain coefficients.

Proof. Considering the following CLF $V(\mathbf{x}, \widehat{\theta})$,

$$V(\mathbf{x}, \widehat{\boldsymbol{\theta}}) = V_1 + \frac{1}{2}e_2^2 + \frac{1}{2}\mathbf{e}_\theta^T \Gamma^{-1} \mathbf{e}_\theta, \tag{24}$$

and the time derivative $\dot{V}(\mathbf{x}, \widehat{\theta})$ is given as

$$\dot{V}(\mathbf{x}, \widehat{\boldsymbol{\theta}}) = \dot{V}_1 + e_2 \dot{e}_2 + \mathbf{e}_\theta^T\left(\Gamma^{-1}\dot{\widehat{\boldsymbol{\theta}}} - \psi_2 e_2\right). \tag{25}$$

As, from (15), $\dot{V}_1 + e_2\dot{e}_2 = \dot{V}_2 < 0$, it remains to find the condition for which $\mathbf{e}_\theta^T(\Gamma^{-1}\dot{\widehat{\theta}} - \psi_2 e_2) < \mathbf{0}$. Using the adaptive law (22), we obtain

$$-\mathbf{e}_\theta^T\Psi_2\left(\mathbf{c}^T\mathbf{x} - e_2\right) = \mathbf{e}_\theta^T\left[x_2 \;\; \sin\left(x_1 + \delta_0\right)\right]^T\left(\mathbf{c}^T\mathbf{x} - e_2\right) < \left|\mathbf{e}_\theta^T\right|\left[\left|x_2\right| 1\right]^T\left(\mathbf{c}^T\mathbf{x} - e_2\right). \tag{26}$$

Using condition (23), it follows that $\dot{V}(\mathbf{x}, \widehat{\theta}) < 0$, $\forall \mathbf{x} \in \mathbb{X}$, and $\forall \widehat{\theta} \in \mathcal{P}$, where $\mathbb{X}$ and $\mathcal{P}$ denote the system's operating and parameters spaces, respectively.

This is the end of the proof. □

4. High-Order Sliding Mode for Exciter Control

For dynamic models (2) and (3) for the exciter and SVC devices, we define the following sliding variables:

$$\begin{aligned} \sigma_e &= V_F - V_{F_{ref}}, \\ \sigma_{svc} &= B_{SVC} - B_{SVC_0}, \end{aligned} \tag{27}$$

where $V_{F_{ref}}$ denotes a field voltage reference, while B_{SVC_0} denotes the initial susceptance of the SVC controller. For designing robust HOSM-based feedback controllers V_t and u_B that provide finite-time convergence of $\sigma_e = 0$ and $\sigma_{SVC} = 0$, the following assumptions are made.

Assumption 5. Both systems (2) and (3) have a well-known defined relative degree r to their tracking output σ.

Assumption 6. In both cases, the following r-sliding set is a nonempty integral set:

$$S = \left\{\sigma = \dot{\sigma} = \ldots = \sigma^{(r-1)} = 0\right\} \neq \varnothing. \tag{28}$$

Assumption 7. A homogeneous r-sliding mode controller u_r can be obtained if there exists a function $U(\sigma, \dot{\sigma}, \ldots, \sigma^{(r)})$, which is continuous everywhere except for the set S

Lemma 1 (see [30]). *Let Assumptions 5–7 hold. Local finite-time convergence of the r-sliding mode $\sigma \equiv 0$ can be achieved and maintained by the following homogenous HOSM controller:*

$$\begin{cases} u_r = -Gsat\left[\varphi_{r-1,r}\left(\sigma, \dot{\sigma}, \ldots, \sigma^{(r-1)}\right)\right], \varphi_{0,r} = \sigma, \\ \text{For } k = 1, \ldots, r-1, \\ \varphi_{k,r} = \text{sign}\sigma^{(k)} + \beta_k N_{k,r}\varphi_{k-1,r}, \\ N_{k,r} = \left(|\sigma|^{p/r} + |\dot{\sigma}|^{p/(r-1)} + \ldots + \left|\sigma^{(k-1)}\right|^{p/(r-k+1)}\right)^{(r-k)/p}. \end{cases} \tag{29}$$

The constant p is the least common multiple of the set $1, 2, \ldots, r$, the parameters β_k are the controller parameters, and $\varphi_{k,r}$ and $N_{k,r}$ are intermediate functions (for the proof of Lemma 1, see [30]).

With $u_r = \varphi_{r-1,r}/N_{r-1,r}$ applied as V_t in model (2) and as u_B in model (3), the field voltage V_F and susceptance B_{VSC} converge to their references or desired final values. The successive time-derivatives $\sigma^{(k)}$ $(k = 1, \ldots, r-1)$ in the recursive algorithm (29) are computed using the following robust high-order sliding mode differentiator (see [31]):

$$\begin{cases} \dot{z}_0 = \nu_0, \nu_0 = -\mu_0 L^{1/r}\left|z_0 - \sigma\right|^{(r-1)/r}\text{sign}\left(z_0 - \sigma\right) + z_1, \\ \dot{z}_1 = \nu_1, \nu_1 = -\mu_1 L^{1/(r-1)}\left|z_1 - \nu_0\right|^{(r-2)/(r-1)}\text{sign}\left(z_1 - \nu_0\right) + z_2, \\ \vdots \\ \dot{z}_{r-2} = \nu_{r-2}, \nu_{r-2} = -\mu_{r-2} L^{1/2}\left|z_{r-2} - \nu_{r-3}\right|^{1/2}\text{sign}\left(z_{r-2} - \nu_{r-3}\right) + z_{r-1}, \\ \dot{z}_{r-1} = -\mu_{r-1} L\text{sign}\left(z_{r-1} - \nu_{r-2}\right), \end{cases} \tag{30}$$

where $L > 0$ is a Lipschitz constant and $z_k \equiv \sigma^{(k)}, \mu_k$ denotes the differentiator parameters.

5. Simulation Results

In this section, different scenarios are simulated for desired operating points to demonstrate the effectiveness and robustness of the proposed ADBS-HOSM control scheme. The values of the parameters are as follows: $H = 8s$, $T_H = 5$, $C_H = 1$, $x_d = 1.81, x_d' = 0.17$, $x_{ds} = 0.99$, $E_q' = 1.08\ p.u.$, $D = 5\ p.u.$, and $V_s = 1 p.u.$ The control technique employs two distinct sets of parameters. Adaptive backstepping parameters (i.e., $k_i, \Gamma, \mathbf{c}$) are chosen to ensure a robust transient response with correction for parameter uncertainties. The operating point of the mechanical load (δ, ω, P_e) is regulated using the three gains k_i, while parameter uncertainties are adjusted by $(\Gamma, \mathbf{c})$. The second group of parameters pertains to the h exciter's high-order sliding mode HOSM controller. The gain G is a tuned gain, whereas (β_i, λ_i) are chosen in accordance with the HOSM control paradigm [32].

5.1. Performance and Effectiveness. The proposed ADBS-HOSM control scheme is applied with $\delta_0 = 1.147$ rad (65.73°), $\omega_0 = 314.159\, rad/s$, and $P_e = 0.98397\ p.u.$ as initial conditions and $\delta_0 = 1.0472\, rad\,(60^\circ), \omega = \omega_0$ as the operating conditions. The values of the control parameters are chosen as follows: $k_1 = 40$, $k_2 = 400$, and $k_3 = 250$ for controllers (23); $\Gamma = diag(0.1, 0.1)$ and $\mathbf{c}^\mathbf{T} = (1, 1, 10)$ for adaptive laws (24) and (25); $\beta_1 = \beta_2 = 0.25$ and $G = 0.5$ for HOSM controllers (29) with $r = 3$; and $\lambda_0 = \lambda_1 = \lambda_2 = 0.15$ and $L = 5.10^{-4}$ for HOSM observers (30). Figures 1–4 show the time history of the transient response provided by both the ADBS-HOSM controller and the controller proposed by Wan and Jiang [18].

5.2. Robustness. Measurement noises are a common problem in power systems, reducing their performance and reliability ([4]; Ghahremani and Kamwa, 2011). We consider realistic scenarios where corrupting noises are present in the available outputs for measurement. In this example, white Gaussian noise with a variance of 0.01 is used to mimic the conditions in the situation described in [4]. The robustness of the proposed ADBS-HOSM controller and the IARK

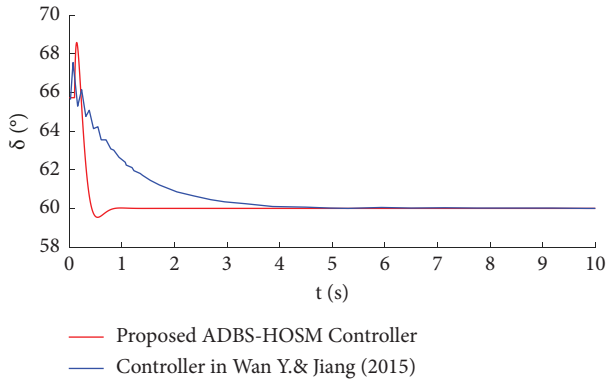

Figure 1: System's response: power angle.

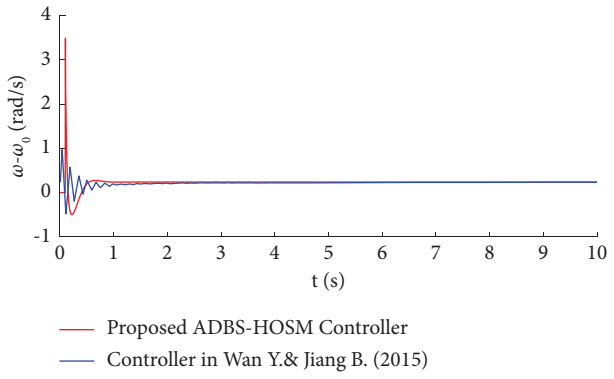

Figure 2: System's response: relative speed.

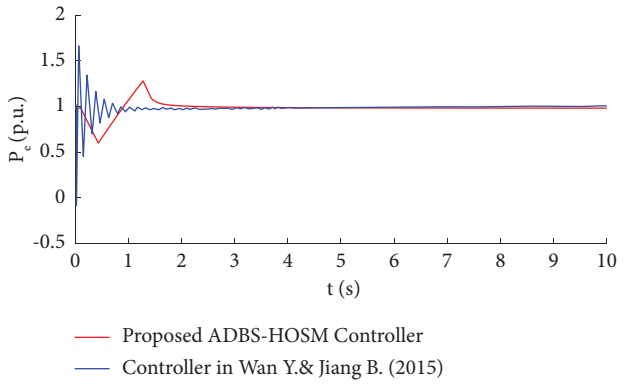

Figure 3: System's response: active power.

controller is compared in Figures 5 and 6. It is clear from this comparison that the ADBS-HOSM controller is superior to the IARK controller in terms of disturbance compensation.

5.3. SMIB-SVC Coordinated Control. In this scenario, the ADBS-HOSM coordinated control scheme is compared to two other recently published coordinated control schemes, the input-output linearization controller (IOL) and the adaptive variable-structure (AVR)/point-synchronous (PSS)/point-integral (PI) controller (SVC) [25, 33]. Figures 7–10 display the results of running the simulation with the same data as in [25]. The simulation results show

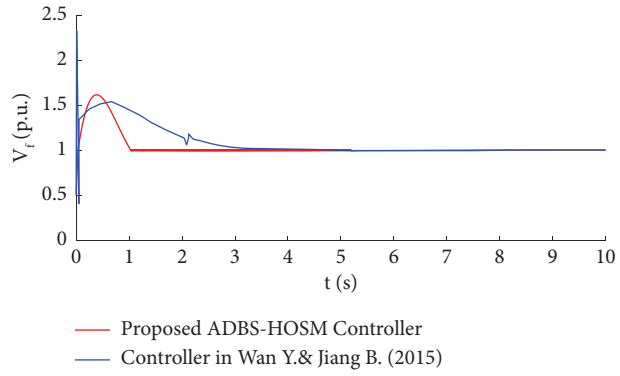

Figure 4: System's response: field voltage.

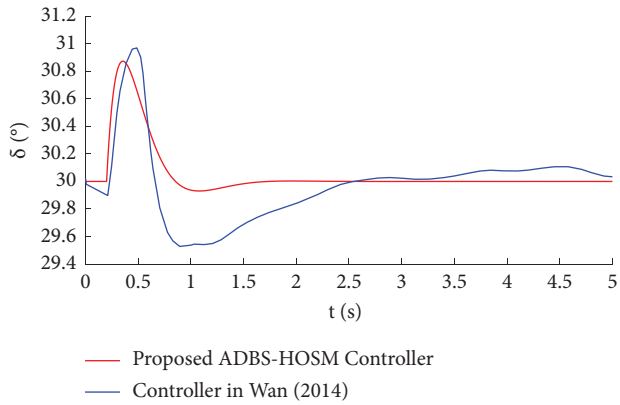

Figure 5: System's response to disturbance: power angle.

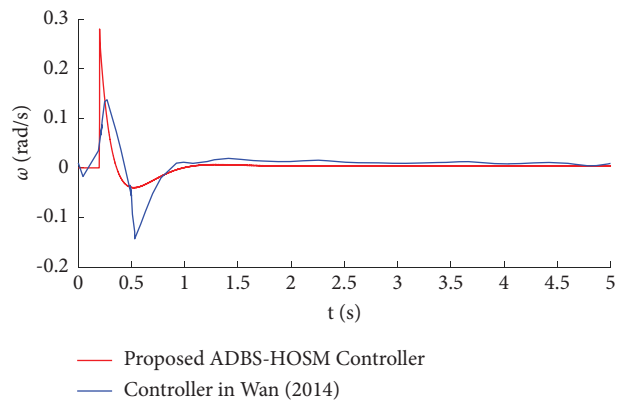

Figure 6: System's response to disturbance: relative speed.

that the proposed coordinate control scheme outperforms those created with traditional control methods like input-output linearization and proportional-integral-derivative (PID). More specifically, ADBS-HOSM improves actuation efficiency in terms of settling time and stability performance.

5.4. Critical Clearing Time and Angle. It is recognized that the size and length of disturbances impact the stability of

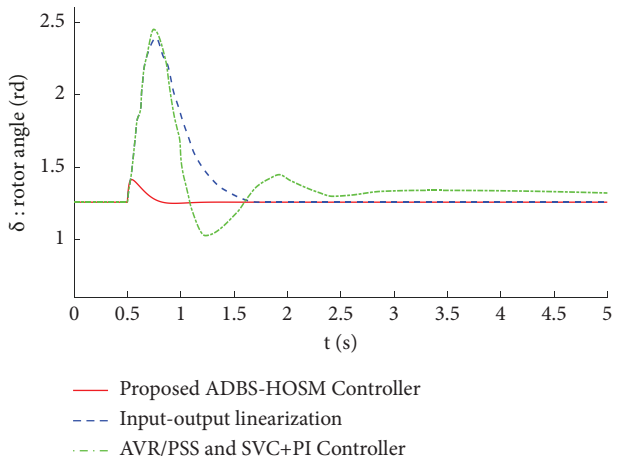

Figure 7: SMIB-SVC coordinated control: power angle.

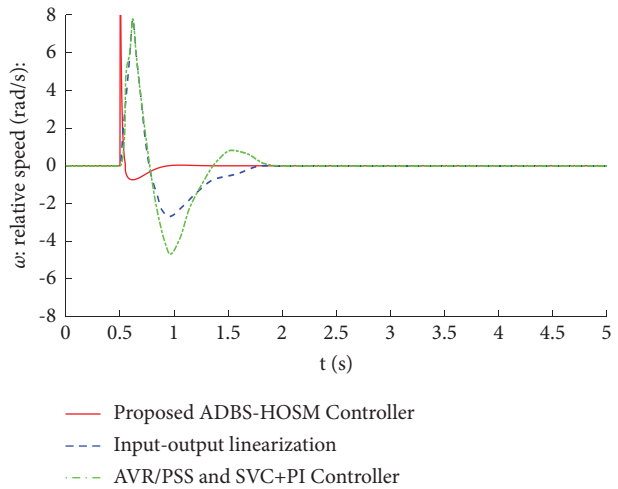

Figure 8: SMIB-SVC coordinated control: SMIB relative speed.

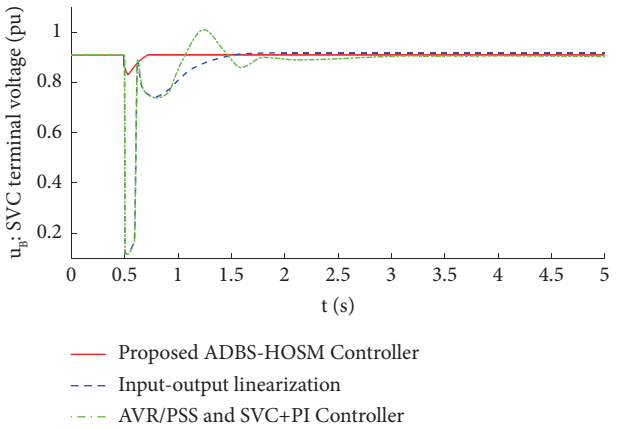

Figure 9: SMIB-SVC coordinated control: SVC Equivalent output.

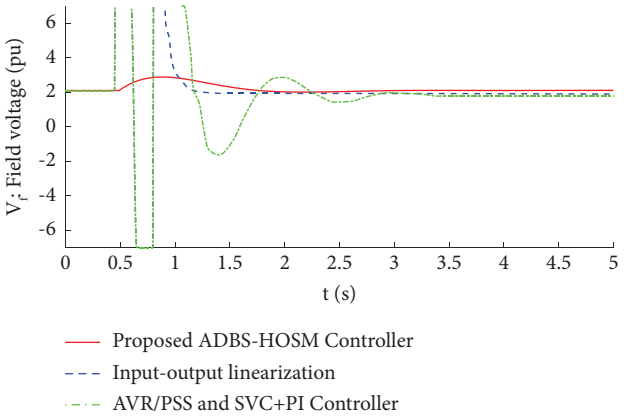

Figure 10: SMIB-SVC coordinated control: SVC Field voltage.

power systems and can lead to synchronization loss. The critical clearing angle δ_{cr} and critical clearing time (CCT) t_{cr} are essential to the power system's stability. Therefore, the defect must be rectified prior to CCT; otherwise, the system will be unstable. The second scenario was resimulated to calculate CCT. As illustrated in Figure 11(a), the system was stable for 0.24 seconds before becoming unstable at 0.25 seconds, as depicted in Figure 11(b). Therefore,

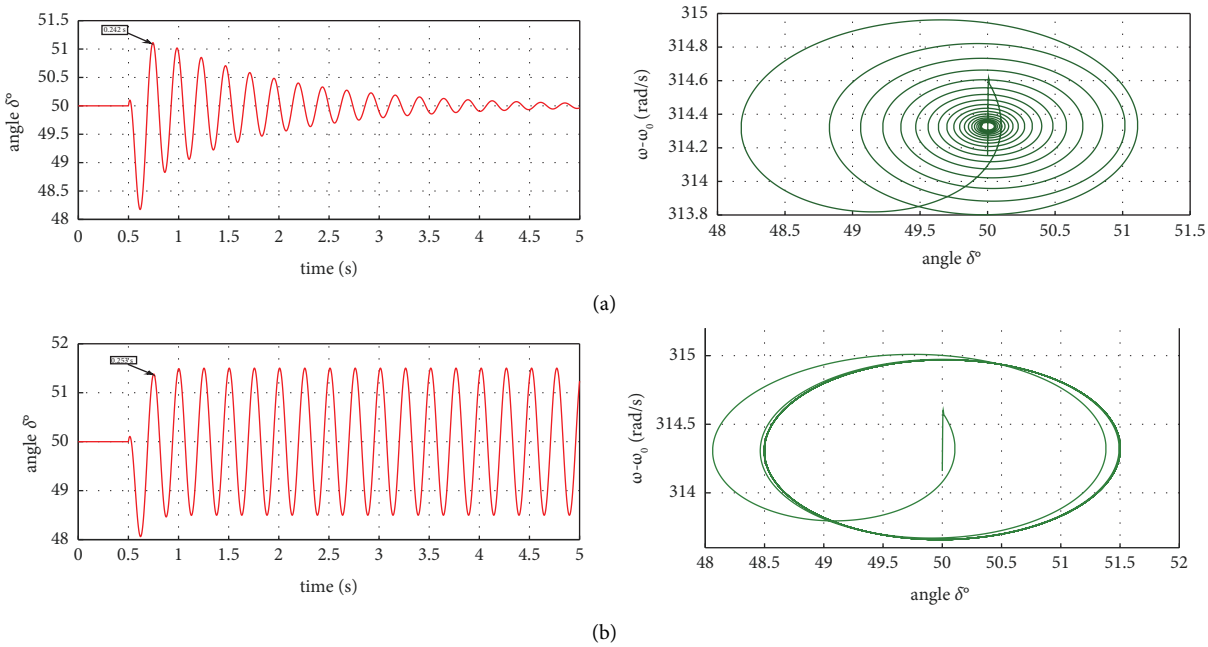

Figure 11: Fault clearing time: (a) before fault clearing; (b) after fault clearing.

0.24 second is regarded as the system's CCT. In addition, the phase-plane frequency angle is presented to check the system's stability.

The four simulated scenarios demonstrate the effectiveness and performance of the presented coordinated SMIB-SVC control strategy. Practical cases, including control in the presence of parameter uncertainties (scenario 5.1), the effect of external disturbances and measurement noises (scenario 5.2), coordination of the SMIB and SVC systems (scenario 5.3), and the critical clearing time and angle (scenario 5.4) were considered. The four scenarios address the essential practical concerns related to the real-time control of modern power systems.

6. Conclusion

A novel robust adaptive control framework was created to simultaneously design an SMIB generator excitation controller with an SVC controller. To provide a robust and implementable controller, uncertainties in physical parameters were considered. Nonlinear controllers were developed for adaptive dynamic backstepping steam-valve load control and high-order sliding mode-based (HOSM) generator excitation control. Using a high-order power model and parameter estimator law, transient stability and voltage regulation were improved. The system's resilience is ensured by the fact that the adaptive control law is designed to adjust for parametric uncertainties, while HOSM is applied to compensate for nonparametric uncertainty, unmodeled dynamics, and external disruptions. Our findings contribute to the existing literature by considering a more realistic damping model of the synchronous generator related to the system's state variables. As a result of our work, the current literature is expanded to include a more realistic damping model of the synchronous generator. The proposed control scheme maintains the nonlinear features of the underlying SMIB-SVC system model by employing high-order modeling. The research findings demonstrated, via simulation, the effectiveness, viability, and superiority of the proposed control scheme in each simulated case. The modular character of the proposed method makes it adaptable to various FACTS devices that can be described in a manner comparable to the one investigated in this study. This can comprise SMIB systems with a static synchronous series compensator (SSSC), a unified power flow controller (UPFC), and a thyristor-controlled reactor (TCR). However, future works can consider some limitations, such as frequency stability for large-scale power systems.

The Kundur and large-scale systems feature a topology with several buses and regions. Both systems can be considered multiload systems, making them appropriate for the multiagent control paradigm. Future works include analyzing the transient response of the entire network and applying the proposed control mechanism to multimachine systems employing FACTS devices. Renewable energy and power grids rely largely on the synchronization and stability of multimachine power systems; hence, employing a multiagent control paradigm, the method will also extend to the distributed coordinated control of networked power systems.

Data Availability

The simulation data used to support the findings of this study are available from the corresponding author upon request.

Conflicts of Interest

The authors declare that they have no conflicts of interest.

Acknowledgments

This project was funded by the Deanship of Scientific Research (DSR) at King Abdulaziz University, Jeddah, under grant no. G-1436-135-504. The authors, therefore, acknowledge with thanks DSR technical and financial support.

References

[1] L. L. Grigsby, *Power System Stability and Control*, CRC Press, Taylor & Francis Group, Boca Raton, FL, USA, 3rd edition, 2012.

[2] M. Momeni and A. H. Mazinan, "Improvement of power quality in grid-connected inverter through adaptation-based control strategy," *Energy, Ecology and Environment*, vol. 4, no. 1, pp. 37–48, 2019.

[3] B. Suman, *Flexible AC Transmission Systems (FACTS)*, CRC Press, Boca Raton, FL, USA, 2018.

[4] Y. Wan, J. Zhao, and G. M. Dimirovski, "Robust adaptive control for a single-machine infinite-bus power system with an SVC," *Control Engineering Practice*, vol. 30, pp. 132–139, 2014.

[5] F. Milla and M. A. Duarte-Mermoud, "Predictive optimized adaptive PSS in a single machine infinite bus," *ISA Transactions*, vol. 63, pp. 315–327, 2016.

[6] C. Liu, B. Wang, and K. Sun, "Fast power system dynamic simulation using continued fractions," *IEEE Access*, vol. 6, pp. 62687–62698, 2018.

[7] R. Bux, C. Xiao, A. Hussain, and H. Wang, "Study of single machine infinite bus system with VSC based stabilizer," in *Proceedings of the 2019 The 2nd International Conference on Robotics, Control and Automation Engineering*, pp. 159–163, Lanzhou, China, November, 2019.

[8] T. K. Roy, M. A. Mahmud, W. X. Shen, and A. M. T. Oo, "An adaptive partial feedback linearizing control scheme: an application to a single machine infinite bus system," *IEEE Transactions on Circuits and Systems II: Express Briefs*, vol. 67, no. 11, pp. 2557–2561, 2020.

[9] N. A. M. Kamari, I. Musirin, and A. A. Ibrahim, "Swarm intelligence approach for angle stability improvement of PSS and SVC-based SMIB," *Journal of Electrical Engineering & Technology*, vol. 15, no. 3, pp. 1001–1014, 2020.

[10] A. F. Mijbas, B. A. A. Hasan, and H. A. Salah, "Optimal stabilizer PID parameters tuned by chaotic particle swarm optimization for damping low-frequency oscillations (LFO) for single machine infinite bus system (SMIB)," *Journal of Electrical Engineering & Technology*, vol. 15, no. 4, pp. 1577–1584, 2020.

[11] R. Kumar, R. Singh, and H. Ashfaq, "Stability enhancement of multi-machine power systems using Ant colony optimization-based static Synchronous Compensator," *Computers & Electrical Engineering*, vol. 83, Article ID 106589, 2020.

[12] R. D. Muhammad, S. Makmur, and A. M. Y. Shiddiq, "Optimal design of PSS on SMIB using particle swarm optimization," *Intek (Informatic Technology) Journal Panellation*, vol. 8, no. 1, pp. 91–95, 2021.

[13] H. Abubakr, J. C. Vasquez, T. Hassan Mohamed, and J. M. Guerrero, "The concept of direct adaptive control for improving voltage and frequency regulation loops in several power system applications," *International Journal of Electrical Power & Energy Systems*, vol. 140, Article ID 108068, 2022.

[14] F. R. Badal, S. K. Sarker, Z. Nayem, and S. K. Das, "Robust design of high performance controller for transient stability enhancement of a single machine infinite bus power system," *International Journal of Power and Energy Conversion*, vol. 12, pp. 294–313, 2021.

[15] K. Himaja, T. A. Kumar, and S. T. Kalyani, "Dynamic stability enhancement of SMIB power system with PSS-SVC with LQR optimal control," *Technological Innovation in Engineering Research*, vol. 3, pp. 61–69, 2022.

[16] L. Carvalho, J. R. L. Neto, J. C. Rezende, M. V. S. Costa, E. V. Fortes, and L. H. Macedo, "Linear quadratic regulator design via metaheuristics applied to the damping of low-frequency oscillations in power systems," *ISA Transactions*, vol. 134, pp. 322–335, 2023.

[17] W. Han and A. M. Stanković, "Model-predictive control design for power system oscillation damping via excitation - a Data-driven approach," *IEEE Transactions on Power Systems*, vol. 38, no. 2, pp. 1176–1188, 2023.

[18] Y. Wan and B. Jiang, "Practical nonlinear excitation control for a single-machine infinite-bus power system based on a detailed model," *Automatica*, vol. 62, pp. 18–25, 2015.

[19] Y. Han and X. Liu, "Continuous higher-order sliding mode control with time-varying gain for a class of uncertain nonlinear systems," *ISA Transactions*, vol. 62, pp. 193–201, 2016.

[20] S. Trip, M. Cucuzzella, C. De Persis, A. Ferrara, and J. M. A. Scherpen, "Robust load frequency control of nonlinear power networks," *International Journal of Control*, vol. 93, no. 2, pp. 346–359, 2018.

[21] K. Adirak and M. Ekkachi, "An improved backstepping sliding mode control for power systems with superconducting magnetic energy storage system," *International Journal of Innovative Computing, Information and Control*, vol. 15, no. 3, pp. 891–904, 2019.

[22] A. Dev, S. Anand, and M. K. Sarkar, "Adaptive super twisting sliding mode load frequency control for an interconnected power network with nonlinear coupling between control areas," *IFAC-PapersOnLine*, vol. 53, no. 1, pp. 350–355, 2020.

[23] S. V. Gutierrez, J. De Leon-Morales, F. Plestan, and O. Salas-Pena, "A simplified version of adaptive super-twisting control," *International Journal of Robust and Nonlinear Control*, vol. 29, no. 16, pp. 5704–5719, 2019.

[24] A. Kanchanaharuthai and E. Mujjalinvimut, "A backstepping-like coordinated excitation and SVC controller design of power systems," *WSEAS Transactions on Power Systems*, vol. 12, pp. 115–123, 2017.

[25] S. Keskes, S. Sallem, and M. B. A. Kammoun, "Nonlinear coordinated control design of generator excitation and static var compensator for power system via input-output linearization," *Transactions of the Institute of Measurement and Control*, vol. 43, no. 1, pp. 205–214, 2021.

[26] L. Zhang, A. Zhang, Z. Ren, G. Li, C. Zhang, and J. Han, "Hybrid adaptive robust control of static var compensator in power systems," *International Journal of Robust and Nonlinear Control*, vol. 24, no. 12, pp. 1707–1723, 2014.

[27] Y. Li, D. Yang, F. Liu, Y. Cao, and C. Rehtanz, *Interconnected Power Systems: Wide-Area Dynamic Monitoring and Control Applications*, Springer, Berlin, Germany, 2016.

[28] H. W. Knobloch, *Disturbance Attenuation for Uncertain Control Systems*, Springer, Berlin, Germany, 2014.

[29] N. L. Carothers, *Real Analysis*, Cambridge University Press, Cambridge, UK, 2000.

[30] Y. Shtessel, C. Edwards, L. Fridman, and A. Levant, *Sliding Mode Control and Observation*, Springer, Berlin, Germany, 2014.

[31] A. Levant and M. Livne, "Exact differentiation of signals with unbounded higher derivatives," *IEEE Transactions on Automatic Control*, vol. 57, no. 4, pp. 1076–1080, 2012.

[32] V. Utkin, "Discussion aspects of high-order sliding mode control," *IEEE Transactions on Automatic Control*, vol. 61, no. 3, pp. 829–833, 2015.

[33] S. Keskes, N. Bouchiba, S. Sallem, C. A. Larbi, and M. B. A. Kammoun, "Transient stability enhancement and voltage regulation in SMIB power system using SVC with PI controller," in *Proceedings of the 6th International Conference on Systems and Control (ICSC)*, pp. 115–120, Batna, Algeria, May, 2017.